Porous Carbon Hot Paper

DOI: 10.1002/anie.201409439

Unusual Ultra-Hydrophilic, Porous Carbon Cuboids for Atmospheric-Water Capture**

*Guang-Ping Hao, Giovanni Mondin, Zhikun Zheng, Tim Biemelt, Stefan Klosz, René Schubel, Alexander Eychmüller, and Stefan Kaskel**

Abstract: *There is significant interest in high-performance materials that can directly and efficiently capture water vapor, particularly from air. Herein, we report a class of novel porous carbon cuboids with unusual ultra-hydrophilic properties, over which the synergistic effects between surface heterogeneity and micropore architecture is maximized, leading to the best atmospheric water-capture performance among porous carbons to date, with a water capacity of up to 9.82 mmol g^{-1} at $P/P_0 = 0.2$ and 25 °C (20 % relative humidity or 6000 ppm). Benefiting from properties, such as defined morphology, narrow pore size distribution, and high heterogeneity, this series of functional carbons may serve as model materials for fundamental research on carbon chemistry and the advance of new types of materials for water-vapor capture as well as other applications requiring combined highly hydrophilic surface chemistry, developed hierarchical porosity, and excellent stability.*

Porous carbons are one of the most common classes of porous solids for organic vapor separation. However, owing to their intrinsic hydrophobic surface and wide micropore size distribution, for quite a long time they were not suitable adsorbents in water-vapor capture, particularly atmospheric water capture (AWC, vapor content of around 1 % in air or 10000 ppm, data from NASA),[1] an important topic because of increasing water shortages,[2] or for clean energy systems, such as adsorption heat pumps.[3]

Among current technologies, hygroscopic brine solutions and hydrophilic inorganic solids (e.g., silica gels, zeolites)[3] and certain kinds of metal-organic frameworks (MOFs)[3,4] show good performances for AWC. However, the effectiveness of such desiccant materials is often limited by their poor durability and the high energy consumption for their recovery.[4] Considering carbon material's high stability and easy regeneration, researchers have paid great efforts to designing new types of functional carbons through surface decoration and meso-/nanopore engineering, however, an efficient AWC based on nanoporous carbons has not yet been achieved. Moreover, the trapping and confinement of water molecules in nanopores as well as the influences of structural heterogeneity on the formation of primary water clusters in nanopores is still not fully understood.[5]

It has been demonstrated experimentally and theoretically that two effects determine the trapping of water into nanopores of carbon: heteroatom-decorated active sites and the micropore structure.[6] Water capture at low pressure ($P/P_0 < 0.2$, $P_0 = 3080$ Pa or 23.1 mmHg at 25 °C) is determined by surface functional groups, such as O-doped, N-doped polar sites, which can induce and stabilize the dense water phase by the formation of hydrogen bonds.[6f] Even after extensive research, to date, the capture of low-pressure water vapor (e.g., 20 % relative humidity or 6000 ppm) is still relatively low, less than 1 mmol g^{-1} on non-functionalized carbons[7] and less than 4 mmol g^{-1} on modified carbons.[8] The possible reasons for this low capture may be 1) the number of active sites is too small to form the required hydrogen-bonding network between carbon pore walls and the water phase; 2) the unsuitable micropore size fails to enable hydrogen bonds to form between water molecules from the opposite side of the micropore, leading to only a thin covering layer rather than filling of the whole pore with water. Another challenge is the simultaneous enrichment of both microporosity and the number of heteroatom-doped active sites, since normally in carbon preparation both features develop contrarily, that is, increasing the carbonization temperature leads to the development of porosities but a sharply decreased number of heteroatom-doped sites.[9]

Herein, we report a class of novel porous carbon cuboids (PCC) with unusual ultra-hydrophilic properties, over which the synergistic effects between surface heterogeneity and micropore architecture is maximized, leading to the best atmospheric-water-capture performance among porous carbons to date, with a water capacity of up to 9.82 mmol g^{-1} at $P/P_0 = 0.2$ and 25 °C. Structurally, a narrow micropore size

[*] Dr. G.-P. Hao, G. Mondin, T. Biemelt, Prof. S. Kaskel
Department of Inorganic Chemistry
Technische Universität Dresden
Bergstrasse 66, 01062 Dresden (Germany)
E-mail: Stefan.Kaskel@chemie.tu-dresden.de
Dr. Z. Zheng
Department of Materials
ETH Zürich (Switzerland)
S. Klosz, Prof. A. Eychmüller
Physical Chemistry
Technische Universität Dresden (Germany)
R. Schubel
Professur für Makromolekulare Chemie
Technische Universität Dresden (Germany)
Prof. S. Kaskel
Fraunhofer Institute for Material and Beam Technology
Winterbergstrasse 28, 01277 Dresden (Germany)

[**] We acknowledge the financial support from the Alexander von Humboldt Foundation and the DFG, thank A. Brünner for taking the SEM images (Figure 1 b,c), J.-Q. Mu for drawing the 3D graphic (Figure 3 b), and M. Oschatz, W. Nickel, and V. Bon for helpful discussions.

Supporting information for this article is available on the WWW under http://dx.doi.org/10.1002/anie.201409439.

distribution in the PCC is achieved, around a diameter of 7.6 Å. Chemically, the PCC show an unprecedentedly high number of heteroatom-decorated active sites, with N:C and O:C ratios of up to 1:5 and 2:5, respectively. Even after pyrolysis at 1000 °C in argon the rich surface heterogeneity is maintained to more than 66 %, and the water capture capacity is still up to 5.80 mmol g^{-1}, which is still in a record value among porous carbon materials (even though the surface area is as low as 270 $m^2 g^{-1}$).

The unique carbon precursor is synthesized through an ultra-fast coordination (30 s; Video S1 in the Supporting Information) of 4,4′-bipyridine and copper ions in the presence of triblock copolymer (F127) in a water/ethanol solution and then collected by centrifugation (Figure 1 a). The introduction of F127 was intended to ensure the as-formed polymer colloids are well dispersed. During this fast reaction, a lone pair of electrons from the heterocyclic nitrogen atom of 4,4′-bipyridine is donated to a copper cation,[10] resulting in the formation of a coordination complex network with the theoretical composition of $CuC_{10}H_8N_2Cl_2$. Subsequently, the copper species easily separate from the nitrogen-containing backbones as carbonization proceeds, leaving nitrogen heterocyclic rings fusing and stacking around the residual copper species. The microporosity is created by leaching the copper species with an oxidative acid, for example, 4 M HNO_3, through which a high number of oxygen-functional groups can be introduced simultaneously.

The SEM images (Figure 1 b,c) show that the uniform and hierarchically porous carbon cuboids of PCC-1, carbonized at 500 °C, are randomly aggregated and overlapped with each other, with a highly rough surface and many macroporous holes distributed all over the particles. The TEM images in Figure 1 d,e reveal the highly amorphous structure of PCC-1. Short and uniform graphene multilayers with a thickness of 2–3 nm are randomly packed and interconnected, between them rich microporosity arises.

Nitrogen physisorption measurements (Figure 2 a) were performed to evaluate the pore structure of PCC-1. The type I isotherm indicates the microporous properties of the material, while the abrupt increase in the high relative pressure region ($P/P_0 > 0.9$) indicates the existence of macropores, which is consistent with the SEM observation. Further, the semi-logarithmic plot of the isotherm (Figure S1 a) reveals a sharp micropore filling with nitrogen molecules in the low-pressure regime ($P/P_0 \approx 2 \times 10^{-5}$), revealing the existence of many micropores with a narrow size distribution. The apparent surface area based on Brunauer-Emmett-Teller (BET) theory ($0.05 < P/P_0 < 0.18$) is 826 $m^2 g^{-1}$, and total pore volume at $P/P_0 =$ 0.9 is 0.45 $cm^3 g^{-1}$. The peak pore size distribution on the basis of non-localized density functional theory (NLDFT) is around 7.6 Å, whose reliability is in turn demonstrated by a good fitting between the simulated adsorption isotherm based on NLDFT theory using the carbon slit pore model and the experimental data (Figure S1 b). Also the high uptake (5.3 mmol g^{-1}, Figure 2 b) of CO_2 at 0 °C over PCC-1 further confirms the existence of rich microporosity, which is consistent with the nitrogen sorption data and the TEM observation.

The sorption kinetics of PCC-1 are evaluated by the InfraSORP technique (Figure 2 c), where an infrared sensor immediately records the temperature increase of the adsorbent arising from the released heat of adsorption, when the probe adsorbate (typically *n*-butane at 1 bar) is introduced into the samples.[11] The sharp temperature increase is related to the adsorption of *n*-butane molecules in the micropores, as these have a much higher adsorption potential than the larger pores. For PCC-1 only 42 % of the adsorbed molecules can be desorbed by an inert gas

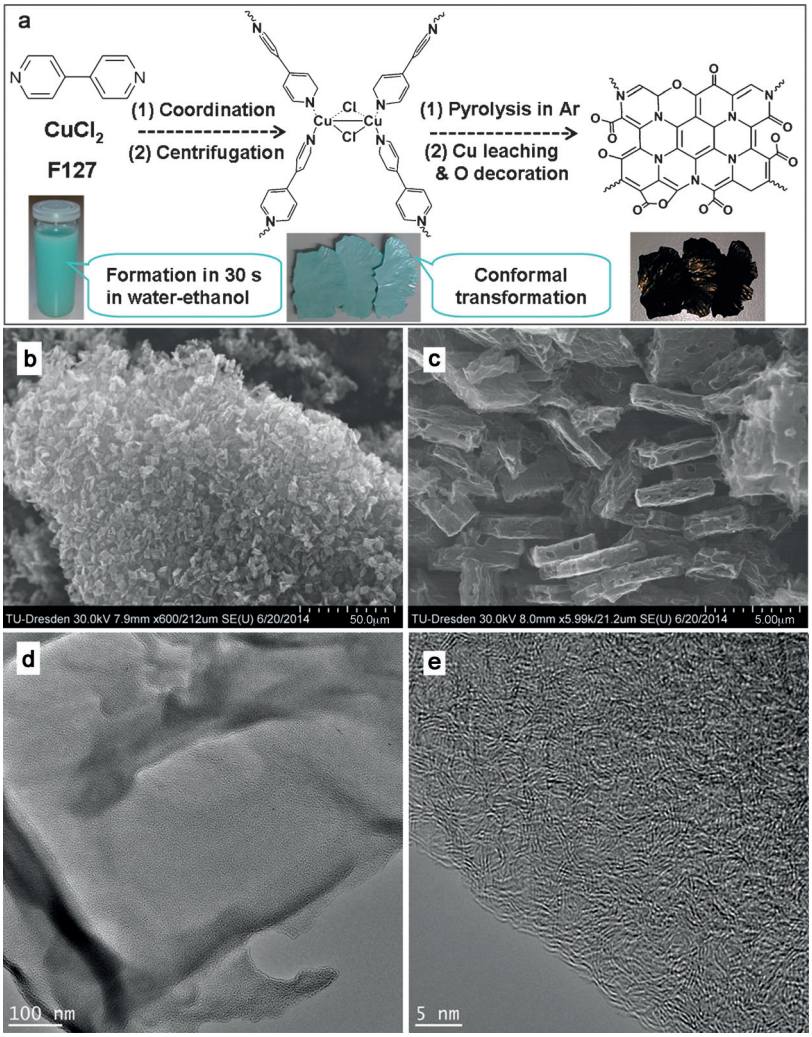

Figure 1. a) synthesis of porous carbon cuboids; b,c) SEM images and d,e) TEM images with low and high magnification of PCC-1. Conformal transformation: During pyrolysis, the morphology of the carbon precursor is well maintained macroscopically and microscopically.

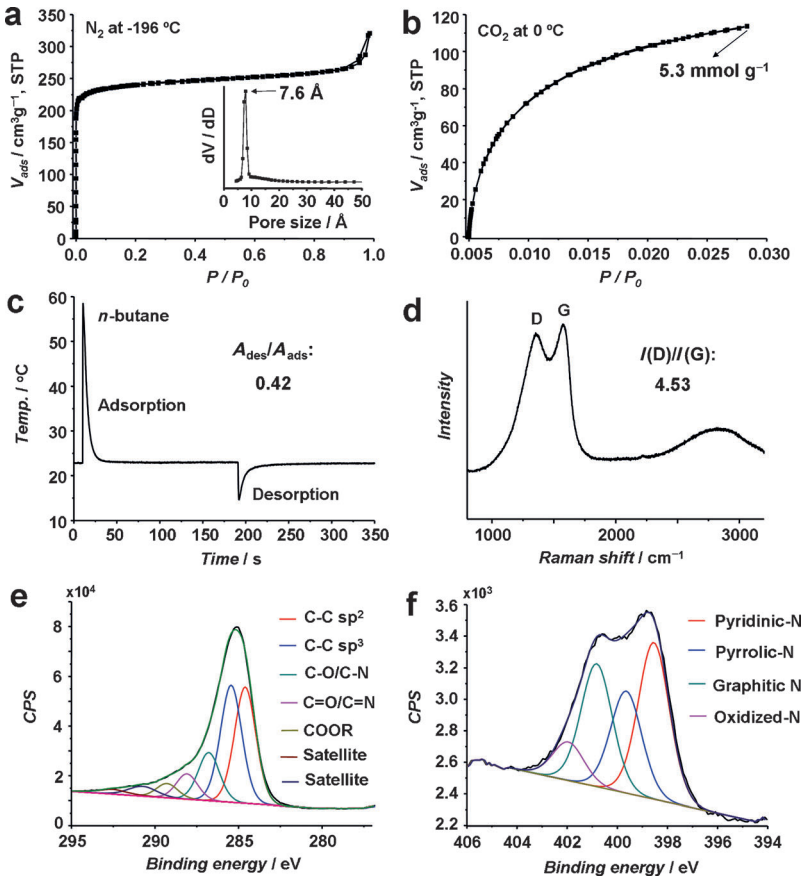

Figure 2. Structural characterization of PCC-1: a) N_2 isotherm and its pore size distribution (inset); b) CO_2 sorption at 0 °C; c) the kinetics evaluation by InfraSORP techniques using *n*-butane as the probe molecule; d) Raman spectrum; e,f) XPS spectra of C1s and N1s.

flow of 120 s, which is much less than for non-doped carbons with similar pore size distribution,[12] indicating the strong trapping effects of PCC-1's heteroatom-decorated narrow micropores, which is confirmed by the similar performance in the successive 10 cycles (Figure S2).

The Raman spectrum of PCC-1 (Figure 2d) shows two peaks around 1578 (G band) and 1357 cm^{-1} (D band). The G band located at 1578 cm^{-1} is attributed to symmetric bond stretching of all the sp^2 carbon atoms while the D band at 1357 cm^{-1} is due to the breathing modes of sp^2 atoms in rings, which is directly related to defects or disorder.[13] The I_D/I_G area ratio is 4.53 for PCC-1 (fitting details in Table S2), indicating its amorphous nature and the presence of many defects arising from the high doping level of N and O atoms.

The surface elemental composition and chemical status of the elements in PCC were measured by X-ray photoelectron spectroscopy (XPS, Table 1, Figure 2e,f, Figure S3–6), while the bulk compositions were determined by elemental analysis (Table 1). For PCC-1, the peaks located at around 285, 399, and 532 eV in the XPS survey (Figure S3) correspond to three characteristic peaks of C1s, N1s, and O1s, with the atomic content of 60 atm% C, 14 atm% N, and 26 atm% O, respectively. The N:C ratio is 0.23, which is even higher than that in the 4,4′-bipyridine molecules (N:C = 0.2), indicating a high transfer rate of nitrogen atoms. The ratio of sp^2 (34.1%) to sp^3 (34.3%) carbon atoms is nearly 1:1, and the content of carbon atoms bonded to N or O atoms is more than 30%. These facts again reveal the amorphous and heterogeneous nature of PCC-1, which is consistent with the Raman results. Furthermore, the amount of N bonded to two sp^2 carbon atoms in a graphene layer, that is, pyridinic-N and pyrrolic-N are 37.2% and 24.3%, respectively, while the content of graphitic-N bonded to three sp^2 carbon atoms is 29.3%. The nitrogen atom at such sites has a lone pair of electrons, which make it more polar, and thus it can preferentially induce the formation of water clusters by hydrogen bonding.[14] For the bulk phase, the C, N, and O atomic content is 61, 13, and 27% for PCC-1, respectively, which is very close to the surface compositions, indicating the uniformity of the atom distribution over the whole sample. Surprisingly, after pyrolysis at 700 °C (PCC-2) the N:C and O:C ratios are still over 0.17 and 0.34 (N and O content of 11 and 23%), and are even over than 0.13 and 0.29 (N and O content of 9 and 21%) after pyrolysis at 1000 °C (PCC-3) (Table 1, Figure S4, S5). These values are much higher than that of other synthetic carbons after 1000 °C pyrolysis.[15]

Thermodynamically and kinetically, the low-pressure water capture may greatly benefit from the N- and O-decorated surface, the numerous and narrow micropores, and the hierarchical and well-defined morphology. The water physisorption isotherms (Figure 3a) show a sharp water capture until $P/P_0 = 0.2$, with a high uptake of 9.82 mmol g^{-1}. This outperforms the widely used commercial and well-researched carbons, which normally adsorb only a negligible amount of water at such low pressure. For example, on commercial BPL activated carbon less than 0.04 mmol g^{-1} and on NC100 less than 1 mmol g^{-1}.[7a,b] On carbon nanotube, less than 0.2 mmol g^{-1},[7c–e] and carbide-derived carbon only 0.04–0.2 mmol g^{-1} are adsorbed;[7f] and also lower under 4 mmol g^{-1} on highly porous modified carbons, for example, nitrogen-doped carbon nanofiber (2–

Table 1: Surface and bulk composition of the porous carbon cuboids.

PCC	Surface composition[a]				Bulk composition[b]			
	atom%			(N+O)/C	atom%			(N+O)/C
	C	N	O		C	N	O	
PCC-1	60	14	26	0.67	61	13	27	0.64
PCC-2	62	13	25	0.61	66	11	23	0.51
PCC-3	65	11	24	0.54	70	9	21	0.42

[a] Based on XPS spectra in Figure S3–S5. [b] Based on elemental analysis, and converted from weight percent to atomic percent. The O content is calculated by difference: 100%−C%−N%. To clarify, to enable a good comparison, the hydrogen content is not counted. PCC-1, PCC-2, and PCC-3 were carbonized at 500, 700, and 1000 °C, respectively.

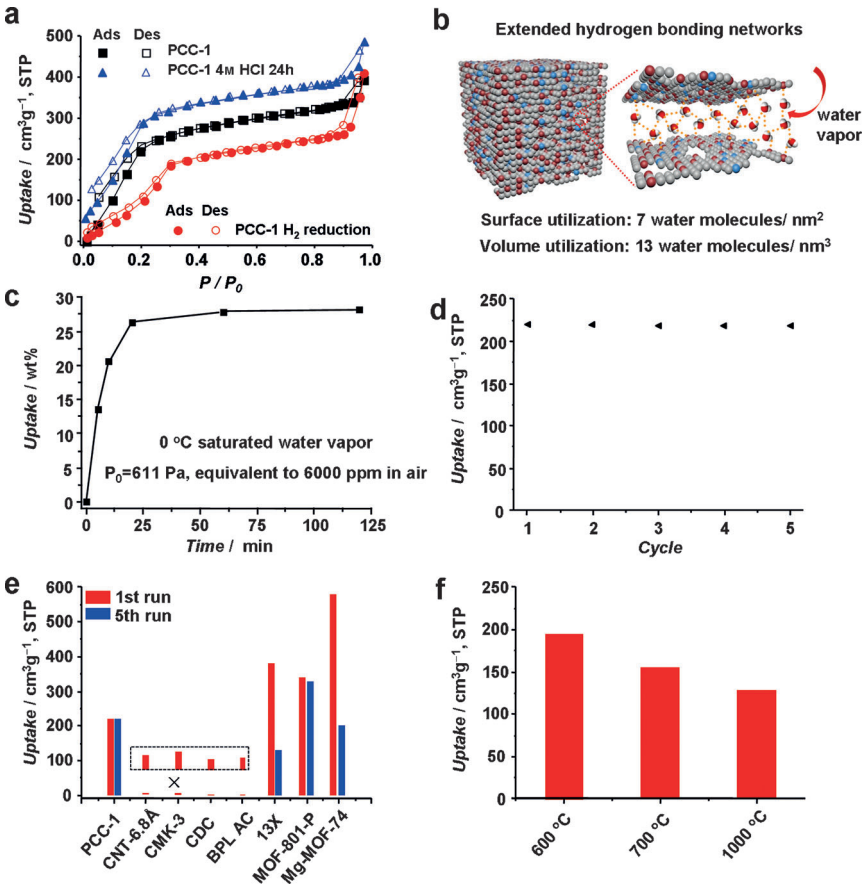

Figure 3. Water-capture performances: a) H_2O adsorption (solid symbols) and desorption (empty symbols) isotherm at 25 °C for PCC-1, PCC-1 after H_2 reduction at 500 °C for 3 h and PCC-1 after immersing in 4 M HCl solution at 25 °C for 24 h, the isotherm for sample after 4 M HCl solution treatment offset vertically by 50 $cm^3 g^{-1}$; b) schematic representation of low-pressure water capture in the PCC micropores: water intermolecular hydrogen bonding and hydrogen bonding between water phase and carbon pore walls; c) time-resolved water sorption at 0 °C; d) 5 cycles of water sorption on PCC-1 at 25 °C, showing the uptake at $P/P_0 = 0.2$; e) water-capture performance of PCC-1 with other best-performing materials reported in literature, such as CNT-6.8 Å,[7d] CMK-3,[7e] CDC,[7f] BPL AC,[7a] zeolite13X,[4b] MOF-801-P[4b] and Mg-MOF-74,[4b] f) the water adsorption uptake at $P/P_0 = 0.2$ and 25 °C of PCCs carbonized at 600, 700, and 1000 °C.

4 mmol g^{-1}),[7a,8a] O-enriched porous carbon (less than 4.4 mmol g^{-1}),[7a] as well as synthetic carbons (less than 2 mmol g^{-1})[8] (Table S1). To our surprise, the sample of PCC-1 before leaching the copper species can deliver an uptake of up to 3.0 mmol g^{-1} at $P/P_0 = 0.2$ (Figure S7a), though its porosity is poorly developed (BET surface area: 58 $m^2 g^{-1}$; pore volume: 0.06 $cm^3 g^{-1}$, Figure S7b). This confirms the ultrahigh polarity of its micropore walls.

Remarkably, 13 water molecules are calculated to be trapped per nm^3 of micropore volume, while seven water molecules are captured per nm^2 surface area of PCC-1 (Figure 3b). These values demonstrate the high efficiency of the highly heterogenized microporosity as a "H_2O reservoir". The N- and O-doped active sites are dispersed at the molecular level so that for every 100 carbon atoms, 60 are N or O doped, thus a "physical picture" can be imagined in which a large number of hydrogen bonds to the doped carbon surface stabilizes the water phase which intern forms an extended intermolecular hydrogen bonding network. Furthermore, we reduced PCC-1 with H_2 at 500 °C, a technique with which most surface functional groups decorating the edges can be removed. In this way, by comparing the isotherm of PCC-1 before and after H_2 reduction, we estimated that the contribution of stable heterogeneity (mainly graphitic-N that is bound into the graphene layer) to the water uptake is still high, up to 50 % at $P/P_0 = 0.2$ (Figure 3a). The abundant narrow micropores can also enhance the dispersion interactions between the water phase and the pore walls.[6g] These factors together contribute to the high utilization of the porosity of the PCCs. Kinetically, we tested the water capture rate at 0 °C based on a gravimetric method (Figure S8). The adsorption of water proceeds rapidly in the first 30 min and then reaches equilibrium, with an uptake of 27.9 wt % (15.5 mmol g^{-1}; Figure 3c), indicating fast sorption kinetics.

For solid desiccants, besides a high capacity and rapid kinetics, the durability is also a critical attribute required for an efficient AWC. As expected, the water-capture capacity is well retained after five equilibrium adsorption–desorption cycles (Figure 3d). Such high-performance is unique among the reported carbons, such as activated carbons,[7a,b] CNTs,[7c,d] mesoporous carbon CMK-3,[7e] carbide derived carbons,[7f] and superior to zeolites and most MOFs (particularly multi-cycling performances), even comparable to the best-performing MOFs, such as MOF-801-P.[4b] The good stability of PCC-1 is further exhibited by a stable performance over 20 adsorption–desorption runs at 0 °C (Figure S9). The regeneration (over 95 % capacity) can be achieved at 100 °C under vacuum for 1 h or in argon flow (40 mL min^{-1}) at 80 °C for 2 h. More importantly, the PCC materials show remarkable chemical stability and thermal stability. For example, the PCC-1 after immersion in 4 M HCl solution for 24 h shows a capacity of 10.4 mmol g^{-1} at $P/P_0 = 0.2$, which is even higher than that of the untreated PCC-1 (Figure 3a). The water-capture capacity at $P/P_0 = 0.2$ is 88 %, 72 %, and 59 % on samples after the pyrolysis at temperatures of 600, 700, and 1000 °C, respectively (Figure 3f, Figure S10). The morphology did not show visible changes (Figure S11, S12), whereas the surface area and porosity decrease significantly as a result of the increasing degree of graphitization (Figure S13, S14, Table S2), for example, a 67 % reduction of surface area can be seen after 1000 °C pyrolysis from 826 to 270 $m^2 g^{-1}$. The important role of the N-/O-doped active sites are further highlighted by comparing the loss of porosity (67 %) and the

remaining water capture capacity (59%, 5.8 mmol g^{-1}). In addition, the microstructure of this PCC series can be easily tuned from micron-sized carbon cuboids into three dimensional networks in the form of thin films or monoliths with greatly shortened building units (100–200 nm), but the water vapor capture capabilities can be maintained or even enhanced (Figure S15 and S16).

In summary, a new class of ultra-hydrophilic porous carbon cuboids have been prepared, through a coordination reaction followed by carbonization, which shows a high density of narrow micropores and surface heterogeneity. Benefiting from such characteristics, a high uptake, fast kinetics, as well as long cycling stability is observed for low-pressure water-vapor capture, which is unusual among carbons and even comparable to the best-performing MOFs with rich microporosity and abundant functional groups. We believe this unique class of functional carbon materials will have a major impact on carbon chemistry and on the advancement of new types of materials for low-pressure water capture from air and other applications requiring highly hydrophilic surface chemistry. Moreover PCC-1 could be developed as a valuable catalyst support material for impregnation from aqueous solutions and with a high affinity to charged metal precursors.

For future work, the PCC-1 material derived from such novel coordination complex networks, with its unique ultra-hydrophilic surface chemistry, high heteroatom doping features and high density of narrow micropores, is named DUT-108 (DUT = Dresden University of Technology). Studies regarding its further application as a metal-free catalyst in the oxygen reduction reaction (ORR) for fuel cells, as catalyst supports, as well as in adsorption heat pumps are underway.

Received: September 25, 2014
Revised: November 3, 2014
Published online: December 17, 2014

Keywords: carbon · doping · microporous materials · nitrogen · water-vapor capture

[1] NASA Earth Fact Sheet: http://nssdc.gsfc.nasa.gov/planetary/factsheet/earthfact.html.

[2] a) E. Kang, G. S. Jeong, Y. Y. Choi, K. H. Lee, A. Khademhosseini, S. H. Lee, *Nat. Mater.* **2011**, *10*, 877–883; b) H. Yang, H. Zhu, M. M. R. M. Hendrix, N. J. H. G. M. Lousberg, G. de With, A. C. C. Esteves, J. H. Xin, *Adv. Mater.* **2013**, *25*, 1150–1154.

[3] a) S. K. Henninger, F. Jeremias, H. Kummer, C. Janiak, *Eur. J. Inorg. Chem.* **2012**, 2625–2634; b) S. G. Wang, R. Z. Wang, X. R. Li, *Renewable Energy* **2005**, *30*, 1425–1441.

[4] a) P. Küsgens, M. Rose, I. Senkovska, H. Fröde, A. Henschel, S. Siegle, S. Kaskel, *Microporous Mesoporous Mater.* **2009**, *120*, 325–330; b) H. Furukawa, F. Gándara, Y.-B. Zhang, J. Jiang, W. L. Queen, M. R. Hudson, O. M. Yaghi, *J. Am. Chem. Soc.* **2014**, *136*, 4369–4381.

[5] a) S. Han, M. Y. Choi, P. Kumar, H. E. Stanley, *Nat. Phys.* **2010**, *6*, 685–689; b) H.-J. Wang, X.-K. Xi, A. Kleinhammes, Y. Wu, *Science* **2008**, *322*, 80–83; c) M. H. Factorovich, E. G. Solveyra, V. Molinero, D. A. Scherlis, *J. Phys. Chem. C* **2014**, *118*, 16290–16300; d) T. Ohba, *Angew. Chem. Int. Ed.* **2014**, *53*, 8032–8036; *Angew. Chem.* **2014**, *126*, 8170–8174; e) O. Byl, J.-C. Liu, Y. Wang, W.-L. Yim, J. K. Johnson, J. T. Yates, Jr., *J. Am. Chem. Soc.* **2006**, *128*, 12090–12097.

[6] a) L. Cossarutto, T. Zimny, J. Kaczmarczyk, T. Siemieniewska, J. Bimer, J. V. Weber, *Carbon* **2001**, *39*, 2339–2346; b) N. Qi, M. D. LeVan, *Carbon* **2005**, *43*, 2258–2263; c) D. D. Do, S. Junpirom, H. D. Do, *Carbon* **2009**, *47*, 1466–1473; d) P. Lodewyckx, *Carbon* **2010**, *48*, 2549–2553; e) T. Horikawa, N. Sakao, T. Sekida, J. Hayashi, D. D. Do, M. Katoh, *Carbon* **2012**, *50*, 1833–1842; f) H.-J. Wang, A. Kleinhammes, T. P. McNicholas, J. Liu, Y. Wu, *J. Phys. Chem. C* **2014**, *118*, 8474–8480; g) J.-C. Liu, P. A. Monson, *Langmuir* **2005**, *21*, 10219–10225.

[7] a) P. D. Sullivan, B. R. Stone, Z. Hashisho, M. J. Rood, *Adsorption* **2007**, *13*, 173–189; b) Ref. [6a]; c) T. Ohba, H. Kanoh, K. Kaneko, *J. Am. Chem. Soc.* **2004**, *126*, 1560–1562; d) Y. Tao, H. Muramatsu, M. Endo, K. Kaneko, *J. Am. Chem. Soc.* **2010**, *132*, 1214–1215; e) M. Thommes, J. Morell, K. A. Cychosz, M. Fröba, *Langmuir* **2013**, *29*, 14893–14902; f) M. Rose, E. Kockrick, I. Senkovska, S. Kaskel, *Carbon* **2010**, *48*, 403–407.

[8] a) Y. Bai, Z.-H. Huang, F. Kang, *Carbon* **2014**, *66*, 705–712; b) Ref. [6f]; c) M. Thommes, C. Morlay, R. Ahmad, J. P. Joly, *Adsorption* **2011**, *17*, 653–661.

[9] a) A. Aijaz, N. Fujiwara, Q. Xu, *J. Am. Chem. Soc.* **2014**, *136*, 6790–6793; b) G.-P. Hao, W.-C. Li, D. Qian, A.-H. Lu, *Adv. Mater.* **2010**, *22*, 853–857.

[10] a) K. Biradha, M. Sarkar, L. Rajput, *Chem. Commun.* **2006**, 4169–4179; b) J. Y. Lu, B. R. Cabrera, R.-J. Wang, J. Li, *Inorg. Chem.* **1999**, *38*, 4608–4611.

[11] a) M. Leistner, W. Grählert, S. Kaskel, *Chem. Ing. Tech.* **2013**, *85*, 747–752; b) P. Wollmann, M. Leistner, W. Graelert, O. Throl, F. Dreisbach, S. Kaskel, *Microporous Mesoporous Mater.* **2012**, *149*, 86–94.

[12] W. Nickel, M. Oschatz, M. von der Lehr, M. Leistner, G.-P. Hao, P. Adelhelm, P. Müller, B. M. Smarsly, S. Kaskel, *J. Mater. Chem. A* **2014**, *2*, 12703–12707.

[13] a) A. C. Ferrari, J. Robertson, *Phys. Rev. B* **2000**, *61*, 14095–14107; b) G.-P. Hao, F. Han, D.-C. Guo, R.-J. Fan, G. Xiong, W.-C. Li, A.-H. Lu, *J. Phys. Chem. C* **2012**, *116*, 10303–10311.

[14] T. Matsuoka, H. Hatori, M. Kodama, J. Yamashita, N. Miyajima, *Carbon* **2004**, *42*, 2346–2349.

[15] a) L. Zhang, Z. Su, F. Jiang, L. Yang, J. Qian, Y. Zhou, W. Lia, M. Hong, *Nanoscale* **2014**, *6*, 6590–6602; b) L. Sun, C. Tian, Y. Fu, Y. Yang, J. Yin, L. Wang, H. Fu, *Chem. Eur. J.* **2014**, *20*, 564–574; c) G.-P. Hao, Z.-Y. Jin, Q. Sun, X.-Q. Zhang, J.-T. Zhang, A.-H. Lu, *Energy Environ. Sci.* **2013**, *6*, 3740–3747.

